

THE CORRELATION BETWEEN H α EMISSION AND VISUAL MAGNITUDE DURING LONG-TERM VARIATIONS IN CLASSICAL BE STARS

T. A. A. SIGUT & P. PATEL

Department of Physics and Astronomy, The University of Western Ontario
London, Ontario, CANADA N6A 3K7

Accepted for publication in *ApJ* January 15, 2013.

ABSTRACT

H α equivalent widths and UBV magnitudes are calculated for Be star disk models that grow in size and/or density with time. We show that these simple models are consistent with the known Be star classes of positive and inverse correlations between long-term variations in H α and V magnitude as identified by Harmanec. We support the conclusion of Harmanec that the distinction is controlled by the inclination of the disk to the line of sight. We demonstrate that the strength of these correlations, particularly those of an inverse correlation where the system becomes fainter as the H α emission strength grows, is strongly influenced by the scale height of the inner Be star disk and the extent of the gravitational darkening of the central B star due to rapid rotation. This dependence may allow coordinated spectroscopic and photometric observations to better constrain these poorly known Be star parameters.

Subject headings: stars: circumstellar matter – stars: emission line, Be

1. INTRODUCTION

Be stars are defined observationally as non-supergiant B stars that have shown emission at least once in the Balmer series of hydrogen (Jaschek et al. (1981); see also reviews by Kogure & Hirata (1982); Slettebak (1988); Porter & Rivinius (2003)). Be stars also exhibit an IR excess relative to that expected from a normal B star (Gehrz et al. 1974; Côté & Waters 1987) and linear continuum polarization of up to 2% (McLean & Brown 1978; Poeckert et al. 1979). All of these observations are consistent with the presence of an equatorial disk of gas surrounding the central B star, an idea (“a nebulous ring of gas”) first suggested by Struve (1931). This basic picture now has ample direct interferometric evidence, and the physical model of a flattened, equatorial disk surrounding the central B star is well established (Dougherty & Taylor 1992; Quirrenback et al. 1993; Stee et al 1995; Quirrenback et al. 1997; Tycner et al. 2005; Stee 2011). About 17% of all non-supergiant B stars in the Milky Way are Be stars, although the fraction varies widely with spectral type, reaching a maximum of $\sim 34\%$ at B1 (Zorec & Briot 1997). Recently, Tarasov & Malchenko (2012) have found that the fraction of early-type Be stars (B0-B3) peaks in Galaxy clusters of ages between 12–20 Myr, suggesting that evolutionary status plays an important role in the Be phenomena. It also seems well established that Be stars are more frequent in lower metallicity environments, such as the Magellanic Clouds (Wisniewski & Bjorkman 2006; Martayan et al. 2006, 2007b, 2010).

Be stars exhibit variability on a wide variety of time scales, from minutes to years/decades (Harmanec 1983; Porter & Rivinius 2003). The origin of short term variability is usually attributed to pulsations within the B star photosphere (Baade 2000; Huat et al. 2009), and there is speculation that pulsations may play a role in the disk formation (Osaki 1999; Cranmer 2009). However,

corotating structures, such as photospheric “clouds,” have also been proposed to explain these variations (Harmanec 1999; Balona 2000). Longer term variations seem connected with the circumstellar disk, either the formation and dissipation of the disk itself, or hydrodynamical processes occurring within the disk, such as spiral density waves which lead to the cyclic V/R variations (Okazaki 1997; Hummel & Hanuschik 1997; Carciofi et al. 2009).

One of the striking aspects of Be stars is episodic creation and destruction of the disk for some Be stars. This is exhibited as a transition in the observed spectrum from a Be star to a normal B star and/or to a Be shell star. Such events present a unique opportunity to study both the structure of the disk and the physical processes responsible for its creation.

Even though the process of disk formation is not well understood, there are observations that seem to show disk formation and dissipation (eg. see Wisniewski et al. 2010). Many Be stars show outbursts, characterized by rapid variability in the emission line profiles. Such variations are normally interpreted as events of rapid, discrete mass ejection (Rivinius et al. 1998a,b), although a definitive observation of material escaping the stellar surface seems lacking (Harmanec, 2012, private communication). These outbursts are thought to be the result of material that is ejected from the star and are mostly seen in early-type Be stars. Stars such as ω CMa (B2IVe), FV CMa (B2IV-Vne), FW CMa (B2Vne), μ Cen (B2Vnpe), η Cen (B1.5Vne) and 28 Cyg (B2.5Ve) are examples of early type Be stars with outburst activity (Rivinius et al. 2001a).

Some Be stars are seen to repeat outbursts regularly. In these cases, the disk is replenished with material every few months to few years, and the outbursts fill up the inner region of the disk with the material. If an outburst is not followed by another one soon, the material falling back on the star, or propagating outwards in the disk, will create a low density region near the star. The

longer the time before the next outburst, the emptier the region becomes. This empty region between the star and the inner edge of the disk makes the disk structure look more like a ring (Meilland et al. 2006). This “inside-out” mass loss can be seen in many stars, for example η Cen (Rivinius et al. 2001a), 60 Cyg (Wisniewski et al. 2010), and 28 CMa (Štefl et al. 1995), where observers measure the variability of the width at the base of the emission lines and/or spectropolarimetric data.

Clark et al. (2003) give observations for o And (B6IIIpe) which show the formation and destruction of the disk in an inside-out manner. In their 15 year data set, the star goes from a normal B star to a Be shell star and back to normal B star, with the cycle repeating. This transition takes around 700 days. Short term outbursts have been noticed which replenish the disk with more material. Clark et al. (2003) model one of the shell episodes, and it is concluded that there is a decrease in density in the innermost regions of the disk. This decrease is shown to slowly propagate outward, indicating an inside-out mass loss in the disk.

Why some B stars, and not others, become Be stars is currently unclear. Rapid rotation of the central B star seems to play a key role (Porter & Rivinius 2003), but details are still lacking as a definitive determination of the actual rotation rates of the central stars is complicated by the potential effects of gravitational darkening (Townsend et al. 2004; Cranmer 2005; Fremat et al. 2005). The evolutionary status of the central B star may also play an important role (Ekström et al. 2008; Tarasov & Malchenko 2012).

Also unclear is the exact mechanism(s) that creates Be star disks. Keplerian rotation, now established for Be star disks (Hummel & Vrancken 2000; Oudmaijer et al. 2008), suggests viscous accretion as the correct physical process (Lee et al. 1991; Porter 1999), but how material is fed into the inner edge of the disk is unknown (Cranmer 2009; Krtićka et al. 2011). It is possible pulsation plays the critical role (Cranmer 2009), and there is tantalizing observational evidence supporting this view (Rivinius et al. 1998; Huat et al. 2009). The role of binarity in the Be phenomena is also unclear (Porter & Rivinius 2003; Tarasov & Malchenko 2012), although the majority of Be stars do not seem to be the result of binary evolution (Baade 1992; Van Bever & Vanbeveren 1997).

2. OBSERVED $H\alpha$ AND UBV CORRELATIONS

Harmanec (1983) describes two classes of long-term variation for Be stars that can be established from contemporaneous observations of photometry (such as visual magnitude and UBV colours) and a measure of the $H\alpha$ emission strength (such as its equivalent width or peak continuum contrast): positive correlations and negative or “inverse” correlations. The distinction between positive and inverse correlations is thought to be geometric (see Harmanec 1983), as will be described shortly.

A positive correlation is seen for most Be stars for which the relevant observations are available, and it is characterized by a decrease in the (visual) magnitude of the system with increasing strength of the Balmer $H\alpha$ emission (such as an increase in its equivalent width in emission). In a $(U - B)$ vs. $(B - V)$ colour-colour diagram, Be stars with a positive correlation change their

luminosity class but not their spectral type (Harmanec 1983). Increasing $H\alpha$ signifies an increasing disk, and it therefore seems natural to expect an increase in the overall brightness of the system, star-plus-disk, as the disk is built.

Many stars are known to exhibit this positive correlation: κ Dra (B6IIIpe; Saad et al. 2004; Juza et al. 1994), 60 Cyg (B1Ve; Koubsky et al. 2000), OT Gem (B2Ve; Božić et al. 1999), V442 And (B2IVe; Božić et al. 2004), EW Lac (B3IVe; Floquet et al. 2000), π Aqr (B1Ve; Nordh & Olofsson 1977), QR Vul (B3Ve; Pavlovski et al. 1983), μ Cen (B2Vnpe; Dachs et al. 1992), ϕ Per (B2Ve; Božić et al. 1995), γ Cas (B0IVe; Doazon et al. 1983), 28 Tau (B8IVev; Hirata et al. 2000; Tanaka et al. 2007), and ω CMa (B2IVe; Harmanec 1998).

On the other hand, an inverse correlation, as described by Harmanec (1983), is characterized by an increase in the magnitude of the system with an increase in the strength of the Balmer emission. In the $(U - B)$ vs. $(B - V)$ colour-colour diagram, Be stars that show an inverse correlation move along the main sequence, changing their spectral type, but not luminosity class (Harmanec 1983).

Fewer stars are known to exhibit this inverse correlation: 4 Her (B9e; Koubsky et al. 1997), 88 Her (B7pshe; Doazan et al. 1982), V1294 Aql (B0Ve; Horn et al. 1982), and η Cen (B1.5IVne; Štefl et al. 1995).

An inverse correlation is thought to occur when a Be star disk is viewed more edge-on (i.e. at higher inclination angle i) (Harmanec 1983). The forming disk can then act to reduce the brightness of the system by blocking the light from the stellar disk, while the small projected area of the disk on the sky keeps the disk emission to a minimum. If the critical inclination angle required to observe an inverse correlation is large enough, inverse correlations will be statistically less likely to be found than positive correlations.

Hence the basic picture is that for Be stars observed at $i < i_{\text{crit}}$, disk formation should result in a positive correlation, while Be stars observed at $i \geq i_{\text{crit}}$ should exhibit an inverse correlation. Of course, i_{crit} may depend on spectral type and/or the particulars of how the disk is being built. However, i_{crit} must depend to some extent on the thickness of the disk. Hence relative numbers of positive and inverse correlations may be able to constrain, in a general sense, the thickness of Be star disks. In fact this argument was used originally by Harmanec (1983) who noted that the occurrence of positive and inverse correlations in the long-term variability was, at the time, among the strongest arguments for flattened Be star disks. This conclusion is strengthened by consistency of the correlation classification: if the record of observations for a given Be star is long enough, the same type of correlation (positive or inverse) will be repeated (Harmanec 2000). As the probability of observing a Be star with inclination i is just $\sin i di$, the probability of observing an inclination $i \geq i_{\text{crit}}$ is $\cos i_{\text{crit}}$. Using the number of cited positive and inverse correlations above, 4 out of 16 Be star systems show an inverse correlation suggesting $i_{\text{crit}} \sim 75^\circ$. However, this is only suggestive because the stars used to estimate the fraction were not selected from a homogeneous sample but simply culled from the literature.

To date there have been no systematic calculations

demonstrating these correlations, either positive or negative, as a function of viewing angle i . Of particular interest is the case of inverse correlation. At high inclination angles (i near 90°), the disk is viewed edge-on and the blockage of starlight is caused by the thickness of the disk. While almost all models of Be star disks assume very thin disks with scale heights set by hydrostatic equilibrium, there are few direct constraints of this assumption, and several lines of evidence suggest that the disks may be much thicker (Arias et al. 2006; Zorec et al. 2007b). In addition, the geometry of the inverse correlation, namely blockage of the equatorial regions of the star, suggests that any gravitational darkening of the stellar surface may also play a critical role. Hence the interplay of disk scale height and gravitational darkening may allow new constraints to be placed on these parameters by the detailed study of inverse correlations. It is the purpose of this paper to provide a preliminary investigation of these correlations using radiative transfer models for Be star disks.

3. CALCULATIONS

The thermal structure of the model Be star disks used in this work was computed with the BEDISK code of Sigut & Jones (2007). This code enforces radiative equilibrium in a photoionized, circumstellar disk of a prescribed density structure by including heating and cooling processes for the nine abundant elements (H, He, CNO, Mg, Si, Ca, & Fe), each over several ionization stages. Details of the atomic models and atomic data, as well as an overview of the BEDISK code, are given in Sigut & Jones (2007). The main energy input into the disk is assumed to be the photoionizing radiation from the central star. The older Kurucz (1993) LTE photoionizing fluxes used by Sigut & Jones (2007) were replaced with the newer, non-LTE calculations of Lanz & Hubeny (2007). To compute the H α equivalent widths and UBV magnitudes of the models, the BERAY code of Sigut (2011) was used. In all cases, this modelling approach considers only an isolated Be star and neglects any potential effects of a binary companion which are outside the scope of the current work.

The density structure of the disk as a function of time was assumed to be of the form

$$\rho(R, Z, t) = \rho_o(t) \left(\frac{R_*}{R} \right)^n e^{-\left(\frac{Z}{H}\right)^2}, \quad (1)$$

where R and Z are the cylindrical co-ordinates for the axisymmetric disk, and R_* is the radius of the central B star. The quantities n and $\rho_o(t)$ are adjustable parameters that fix the density structure of the disk. The disk was assumed to extend from the stellar photosphere at $R = R_*$ at the inner edge to an outer disk radius of $R = R_d(t)$. This simple density model has been very successful in interpreting a wide range of Be star observations (Gies et al. 2007; Tycner et al. 2008; Jones et al. 2008). The disk is assumed to be in Keplerian rotation and hence rotationally supported in the R direction.

The vertical (or Z) dependence of Eq. (1) contains the scale height function H which is defined as

$$H = \left(\frac{2R^3 kT_{HE}}{GM_* \mu m_H} \right)^{1/2}. \quad (2)$$

Here M_* is the mass of the central B star, μ is the mean-molecular weight of the disk gas, and T_{HE} is an assumed isothermal disk temperature. The Z -dependence of Eq. (1) and Eq. (2) follow from the assumption that the disk is in vertical hydrostatic equilibrium set by the Z component of the stellar gravitational acceleration and an assumed isothermal disk temperature, T_{HE} . In Eq. (2), the mean molecular weight, μ , was taken to be 0.68, appropriate for a fully-ionized hydrogen gas with a 10% mixture of neutral helium. The isothermal disk temperature, T_{HE} (which is taken to be a constant for the entire disk) is further discussed below.

Eq. (2) can be instructively written as

$$\frac{H}{R} = \frac{c_s}{V_K}, \quad (3)$$

where c_s is the local sound speed in the disk (set by temperature T_{HE}) and V_K is the Keplerian orbital velocity at R . As the radiative equilibrium temperatures in the disk give sound speeds on the order of ten km s^{-1} while the orbital speed is many hundreds of km s^{-1} , the hydrostatic model predicts disks that are very thin, often only few percent of the stellar radius near the star.

Note that T_{HE} is only used in Eq. (2) to fix the vertical density structure of the disk; the actual temperatures in the disk, $T(R, Z)$, are found by enforcing radiative equilibrium. Sigut et al. (2009) consider consistent models in which the vertical structure of the disk is found by integrating the equation of hydrostatic equilibrium in a manner consistent with the radiative equilibrium disk temperatures: this treatment eliminates the need for the parameter T_{HE} . In general, Sigut et al. (2009) find that vertical disk scale heights are generally overestimated by Eq. (2), using the typical value of $T_{HE} \approx 0.6 T_{\text{eff}}$, in the inner regions of the disk due to a cool zone that tends to form in the equatorial plane of the disk near the star for disks of sufficient density (i.e. ρ_0). Nevertheless, as will be shown in a later section, disks using Eq. (2) with $T_{HE} = 0.6 T_{\text{eff}}$ are already sufficiently thin to have significant consequences for the strength of the predicted H α -V magnitude correlations.¹

The thermal disk models are thus described by the spectral type of the central B star (which is assumed to fix the stellar mass, radius and effective temperature) and the parameters in Eq. (1) that fix the density of the disk: ρ_o , the base density (in g cm^{-3}), n , the power-law index, and R_d , the outer disk radius. The isothermal disk temperature used in Eq. (2), T_{HE} , is also a parameter of the models, and variations of this parameter are the subject of Section 4.2.

In the present work, two spectral types were considered for the central B stars: B1V and B5V, representing an early and later-type Be star. The assumed fundamental parameters are given in Table 1. Be stars are, of course, known as rapid rotators and hence the role of gravitational darkening of the stellar photosphere must be considered. This effect will be explicitly considered in Section 4.4.

¹ McGill et al. (2012) demonstrate that the effect of gravitational darkening on the disk temperatures can result in scale heights even smaller than those found by Sigut et al. (2009). Hence the use of Eq. (2) in the current work should be considered an upper limit to the thicknesses of disks in hydrostatic equilibrium.

Table 1
Parameters adopted for the central B stars.

Parameter	B1V	B5V
Mass (M_{\odot})	13.2	5.9
Radius (R_{\odot})	6.4	3.9
Luminosity (L_{\odot})	$1.4 \cdot 10^4$	$6.9 \cdot 10^2$
T_{eff} (K)	25 000	15 000
$\log(g)$	4.0	4.0
T_{HE}	15 000	9 000

Note. — The mass and radius calibrations are taken from Cox (2000).

As this paper is concerned with the optical signature of disk formation and dissipation, some prescription for these processes is required. One-dimensional, hydrodynamic simulations that evolve the disk surface density as a function of time within the framework of viscous accretion have reached a high degree of sophistication (Carciofi 2010; Haubois et al. 2012) and have been impressively used to model specific Be stars in considerable detail (see, for example, Carciofi et al. (2009) for ζ Tau). Carciofi et al. (2012) have recently used the observed decline of the V-magnitude of 28 CMa during a disk dissipation phase to infer a value of $\alpha = 1.0 \pm 0.2$ for the disk viscosity parameter using detailed hydrodynamic and radiative transfer modelling. However this current paper is focused mainly on the geometrical origin of the correlation classes noted in the previous section and the influence of the disk scale height and gravitational darkening of the central stars on these correlations. In addition, the models here are not meant to represent any specific Be star in detail. For these reasons, a very simple model was used to build the disk as a function of time (variations of this basic description are discussed at the end of this section). The overall density of the disk was assumed to linearly increase over a time β to a maximum value of ρ_{max} , namely

$$\rho_o(t) = \rho_{\text{max}} \left(\frac{t}{\beta} \right). \quad (4)$$

The outer edge of the disk was assumed to expand linearly with time with a fixed radial expansion speed v_r as

$$R_d(t) = v_r t. \quad (5)$$

For both spectral types, we took $\rho_{\text{max}} = 10^{-10} \text{ g cm}^{-3}$ and $\beta = 365$ days. For the B1V model, we took $v_r = 5 \text{ km s}^{-1}$ and for the B5V model, we took $v_r = 3 \text{ km s}^{-1}$. These choices ensure that the disk sizes expressed in terms of the stellar radius are the same for both models. Hydrodynamical simulations suggest outflow velocities in viscous disks of a few km s^{-1} (Lee et al. 1991; Porter 1999). In addition, in the density law of Eq. (1), n was taken to be 3.5 and T_{HE} was set to $0.6 T_{\text{eff}}$. The growth of the disk with time for both models is given in Table 2. After one year, the disk around the B1V model reaches 1.05 AU in radius and has a mass of $3.25 \cdot 10^{-9} M_{\odot}$; the B5V model reaches 0.63 AU with a mass of $6.50 \cdot 10^{-10} M_{\odot}$. We note that both of these models result in quite substantial Be star disks, with low-inclination $\text{H}\alpha$ equivalent widths approaching 40 \AA in emission.

Table 2
Disk density and radius as a function of time for the B1V and B5V models.

Time (days)	ρ_0 (g cm^{-3})	R_d (R_{\star})
9.1	$2.5 \cdot 10^{-12}$	1.9
18.2	$5.0 \cdot 10^{-12}$	2.8
27.4	$7.5 \cdot 10^{-12}$	3.6
36.5	$1.0 \cdot 10^{-11}$	4.5
91.3	$2.5 \cdot 10^{-11}$	9.8
127.7	$3.5 \cdot 10^{-11}$	13.4
182.5	$5.0 \cdot 10^{-11}$	18.6
237.3	$6.5 \cdot 10^{-11}$	23.9
273.7	$7.5 \cdot 10^{-11}$	27.5
310.3	$8.5 \cdot 10^{-11}$	31.0
365.0	$1.0 \cdot 10^{-10}$	36.3

Note. — The final disk masses after one year are $3.25 \cdot 10^{-9} M_{\odot}$ (B1V) and $6.50 \cdot 10^{-10} M_{\odot}$ (B5V).

To dissipate the disk as a function of time, an inner hole was evacuated in the final density model of the build phase at $t = 365$ days starting at the inner edge of the disk at $1 R_{\star}$. The outer edge of the hole was assumed to propagate outward at speed v_r so that the disk sizes of Table 2 also represent the outer radii of the evacuated hole at time $t + 365$ days. Inside this hole, the density was reduced by a factor of 10^3 . Thus the mass of the disk is reduced by a factor of 10^3 over the duration of the dissipation phase (one year) and the final density model for both disks was $n = 3.5$ and $\rho_0 = 10^{-13} \text{ g cm}^{-3}$. This density is so low that the $\text{H}\alpha$ line of the model is indistinguishable from the photospheric (absorption) line and the IR excess is $< 1\%$. Thus the assumption is that the disk is lost “inside-out,” a direction consistent with many observations (Rivinius et al. 2001a; Clark et al. 2003; Meilland et al. 2006). The disk mass as a function of time for the B1V model is shown in Figure 1. Note that in the dissipation stage, the sharp density contrast at the outer edge of the evaluated hole was smoothed somewhat to improve the radiative transfer solution there.

The calculation of the $\text{H}\alpha$ line profiles was done with the BERAY code (Sigut 2011). Here the radiative transfer equation is solved along a series of rays through the star-plus-disk system. For rays terminating on the stellar surface, photospheric LTE $\text{H}\alpha$ profiles were computed with the code of Barklem & Piskunov (2003). To obtain the V-magnitude of the system, a visual SED was computed for each model and the V-transmission curve of Johnson (1966) was used.

Only a single BEDISK model is required for the disk-building sequence as the disk can be truncated at the appropriate outer radius in the BERAY code. However, an individual BEDISK model is required for each time in the disk loss sequence. As the disk is evacuated inside-out, the growing size of the inner gap changes the photoionizing radiation field reaching the remaining parts of the disk. Hence a consistent thermal structure for the disk is required in each case, and the temperature structure of the disk changes along the loss sequence. This is further

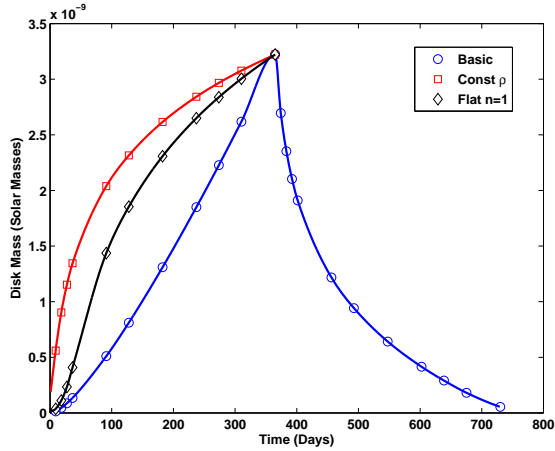


Figure 1. Disk mass as a function of time for the B1V model. The maximum disk mass is $3.25 \cdot 10^{-9} M_{\odot}$ at one year. The circles represent the basic model described by Eqs. (4) and (5). The squares represent the constant ρ_0 model and the diamonds, the flat $n = 1$ model, as described in the text. The disk mass as a function of time for the B5V model is very similar except that the maximum disk mass is $6.50 \cdot 10^{-10} M_{\odot}$ after one year.

discussed in Section 4.2.

In addition to the basic set of disk models described above by Eqs. (4) and (5), two alternate assumptions about the growth of the disk mass during the build phase were considered. In the first variation, Eq. (4) was replaced with the assumption of a constant base density, $\rho_o(t) = \rho_0$, for all times, where ρ_0 was taken to be $10^{-10} \text{ g cm}^{-3}$. In the second variation, the constant density $\rho_o(t) = \rho_0$ assumption was used along with the requirement that in the inner region of the disk where $R \leq 5 R_*$, the power-law index n in Eq. (1) was $n = 1.0$. An index of $n = 3.5$ was retained for $R > 5 R_*$. In this case, to give a model with a final disk mass consistent with the other two models, ρ_0 was set to $2.7 \cdot 10^{-12} \text{ g cm}^{-3}$. Figure 1 compares the disk mass as a function of time in the build phase for these two variations with the basic model previously described. Both of these variations result in much more massive disks at early times but result in the same total disk mass at the end of the disk build phase at 365 days.

4. RESULTS

4.1. Basic Model

To establish a reference set of models, the disks surrounding the stars were assumed to be in strict vertical hydrostatic equilibrium with no gravitational darkening of the central star. For typical stellar parameters, Eq. (2) predicts very thin disks with $(H/R) \sim 0.05$ in the inner regions. In addition, it is well known that Be stars are rapid rotators and hence gravitational darkening is potentially an important effect. This will be discussed in Section 4.4.

As discussed in the Section 2, stars showing a positive correlation show a decrease in visual magnitude with an increase in the equivalent width (EW) of H α . Stars showing an inverse correlation show an increase in visual magnitude with an increase in the EW of H α . For the calculations in this report, instead of the visual magnitude itself, the change in visual magnitude (ΔV) is used which is defined as the difference between the visual magnitude of a given model and the visual magnitude value

for the last model of the disk loss phase at 730 days. As noted in the previous section, this last model shows no evidence of disk emission and can be taken to represent the isolated B star.

Consider first the B1V and B5V models seen nearly face-on at $i = 15^\circ$. Figure 2 shows the disk growth (1 – 365 days) and dissipation (366 – 730 days) phases of both models. Both spectral types behave in a very similar manner. The top panel of the figure shows the change in EW of H α emission line as a function of time,² while the bottom panel shows the change in visual magnitude (ΔV). In the top panel, the H α equivalent width increases with time as the density and the outer radius of the disk increase. It can be seen that the strength of H α reaches its maximum, $\approx 30 \text{ \AA}$, by essentially ~ 100 days, when the outer radius of disk has reached $\sim 10 R_*$ (Table 2). This is consistent with the observed sizes of Be star disks resolved with optical interferometry using H α (Tycner et al. 2005; Grundstrom & Gies 2006). When the disk dissipation stage starts at 365 days, there is a temporary increase in the H α equivalent width for another ~ 15 days before entering a steep decline. This rather counter-intuitive result occurs because the equivalent width is a measure of the strength of H α relative to the local continuum, i.e.

$$\text{EW} \equiv \int \left(\frac{F_\nu - F_c}{F_c} \right) d\nu, \quad (6)$$

where F_ν is the flux at frequency ν and F_c is the flux of the reference continuum. Because of the very large optical depths in H α , it is formed over a wide region of the disk extending out to $\sim 10 R_*$. The optical continuum, on the other hand, forms closer to the star. So in an inside-out dissipation scenario, the strength of the reference continuum is reduced more quickly than that in the line, and this leads to an increase in the equivalent width, even though F_ν declines during this phase. This ‘bump’ is over by ~ 400 days, by which time the inner evacuated zone has expanded to $\sim 3.5 R_*$.

The growth and dissipation phases do not mirror one another because of the inside-out nature of the dissipation. In the growth phase, the base density (ρ_0) and outer radius (R_d) of the disk both grow linearly in time. However, during the dissipation phase, only the extent of the inner evacuated region grows linearly with time, leading to an inner cavity in the disk. By 730 days, the disk has $\rho_o = 10^{-13} \text{ g cm}^{-3}$ and extends to $36 R_*$. This disk is so rarefied that there is essentially no emission due to the disk in H α , and its EW represents the (negative) absorption width of the photospheric line. Note that the first calculated model in the growth phase is after 9 days at which point the disk has grown to $1.9 R_*$. This is the reason the initial equivalent width in the Figure 2 is slightly larger (i.e. affected by emission) than the last model in the dissipation sequence.

The bottom panel of Figure 2 shows the change in the V-magnitude over the growth and dissipation phases. The reference model for the colour differences is chosen to be the last model in the dissipation sequence (730 days) because, as noted above, it exhibits a pure photo-

² We adopt the non-standard convention that a positive EW denotes emission and a negative EW, absorption.

spheric spectrum which is uncontaminated by the disk. The sense of the visual magnitude changes are always brightening in the growth phase and dimming in the dissipation phase (with one brief exception noted below). As the system is viewed nearly face-on, there is little obscuration of the star by the disk, and hence the disk always adds to the brightness of the system. The very rapid decline in the V magnitude of the system at the onset of the dissipation phase reflects the above discussion about the formation of the optical continuum close to the star, within a few stellar radii.

In the correlation classification scheme of Section 2, both models (B1V and B5V) would be an instances of a positive correlation as the system brightens as the disk (and the $H\alpha$ emission strength) grows. Note, however, there would be a brief window of an inverse correlation during the initial phase of the inside-out dissipation, as the system would grow fainter while $H\alpha$ continued to increase during the ‘bump’ between 365 and 380 days.

Another interesting way to look at this sequence of models is in a colour-colour diagram of $(U - B)$ versus $(B - V)$ where UBV are the familiar Johnson photometric colours. The evolution of the entire sequence for the B1V and B5V models is shown in Figure 3. To calibrate the colours, the colours of the last model in the dissipation phase (730 days) were forced to be the colours of a normal B1V or B5V star as tabulated by Fitzgerald (1970). The additive constants were then applied to every model in the sequence. Note that as the first model is after 9 days of disk growth, it will not lie exactly on the main sequence reference point. For both modes, the growth track is from the main sequence, nearly horizontal in the figure, towards the supergiant sequence, resulting in models that have nearly constant $(U - B)$ colours but progressively redder $(B - V)$ colours. The tracks are such that the systems move from the V region, horizontally, towards the Ia region of the colour-colour diagram; this is the observed behaviour for positively correlated systems in which movement in the colour-colour diagram is often categorized as the system “changing its luminosity class between V and Ia without any substantial change of its spectral type” (Harmanec 1983). This behaviour is a reflection of the nature of the additional continuum emission from the disk. Typically, the continuum excess for Be stars grows with longer wavelengths (because it is principally due to free-free emission). Hence the U colour is hardly affected, while the V colour is most affected (as noted above). As the star is essentially unobscured for $i = 15^\circ$, this simple fact gives the horizontal motion in the colour-colour diagram.

We now turn to the same set of models, B1V and B5V, but for a nearly edge-on disk seen at $i = 89^\circ$. In this case, the disk can obscure the star’s photospheric light, and this leads to new effects shown in Figure 4. The top panel shows the change in the $H\alpha$ EW, and it again grows with time as the disk is built. It starts at negative values this time (i.e. net absorption) due to the much weaker disk emission at $i = 89^\circ$ degrees and the effect of shell absorption. The photospheric equivalent widths are represented by the equivalent widths at 730 days. In this series, the $H\alpha$ equivalent width grows steadily with time and reaches a maximum in emission of $\approx 6 \text{ \AA}$ at 365 days. In the edge-on case, the maximum $H\alpha$ EW

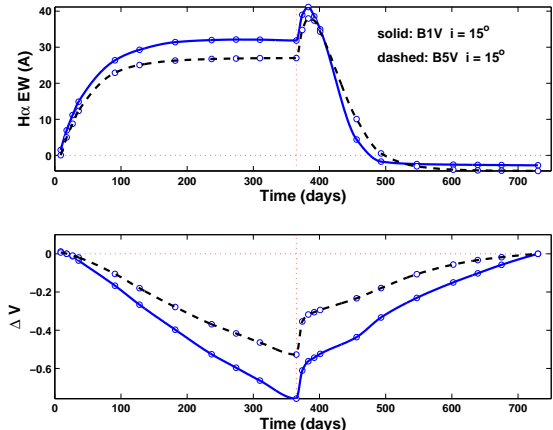


Figure 2. $H\alpha$ equivalent width (\AA , top panel) and change in V -magnitude (bottom panel) as a function of time for the B1V (solid lines) and B5V (dashed lines) models seen nearly pole-on at $i = 15^\circ$. All models assumed a thin, hydrostatic disk with H set by Eq. (2) and gravitational darkening of the central B star was not included. The disk grows for one year and then dissipates over one year as described in the text.

is much smaller than in the face-on case, as expected from the much smaller projected area of the optically thick disk on the sky. The bottom panel shows the effect on the V magnitude. For times less than about 100 days, the system is fainter than the star itself, reflecting the obscuration by the disk. However, the effect is very small (a few hundredths of a magnitude), and this is a direct consequence of the very thin nature of a purely hydrostatic disk.

In the colour-colour diagram corresponding to the $i = 89^\circ$ models (Figure 3), more inclined tracks are seen. In this case, the U colour is affected by absorption by the disk, making it larger and hence $(U - B)$ smaller. Observationally, inversely correlated systems “move along the main sequence changing its spectral but not luminosity class” (Harmanec 1983). This behaviour is clearly reproduced for the B5V model at $i = 89^\circ$ during its disk build phase. However, the B1V model does not move along the main sequence, and this may be related to the very weak inverse correlations predicted by this set of basic models with hydrostatic disks.

4.2. Enhanced Disk Scale Heights

In the previous section, we presented the optical signature of a disk build and dissipation sequence. The case of positive correlation is well represented by the $i = 15^\circ$ models of both spectral types. The overall V magnitude of the system increases by approximately half a magnitude over the build phase of the disk. In addition, the movement in the colour-colour diagram is as observed: towards the giant sequence at nearly constant spectral type.

However, the case of an inverse correlation is less well represented. In the edge-on model, for which an inverse correlation is expected, only a very small magnitude increase is seen during the initial build phase of the disk, amounting to a few hundredths of a magnitude. Observed inversely correlated systems typically show magnitude changes of a tenth of a magnitude or more. Behaviour in the colour-colour diagram is more as observed; there is a tendency to evolve along the main sequence, changing the system’s spectral type.

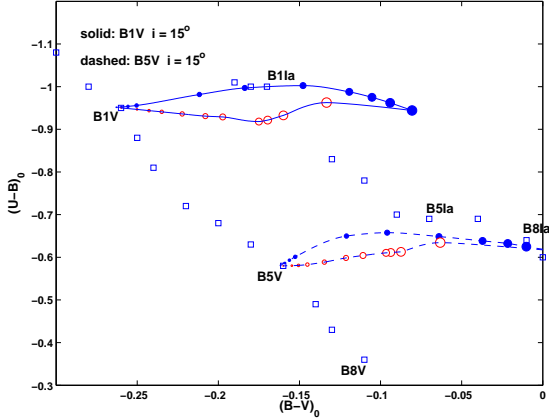


Figure 3. The movement of the B1V (solid lines) and B5V (dashed lines) models in an optical colour-colour diagram as the disk grows (filled blue circles) and dissipates (open red circles). The models assumed a thin, hydrostatic disk and gravitational darkening was not included. The models are viewed nearly pole-on at $i = 15^\circ$. The circles grow and diminish in size following $\rho_0(t)$. The squares are the observed normal (star only) colours for main sequence (V) and supergiant (Ia) stars from Fitzgerald (1970).

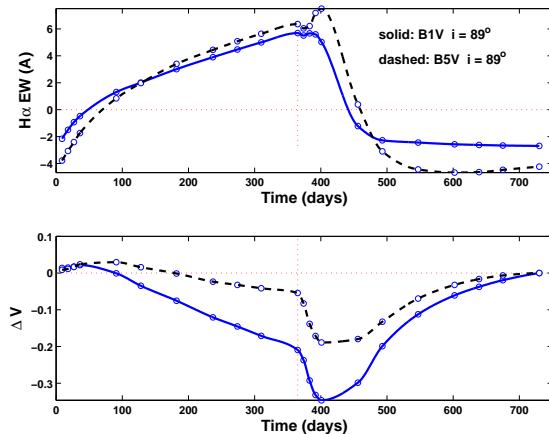


Figure 4. Same as Figure 2 but for edge-on disks seen at $i = 89^\circ$.

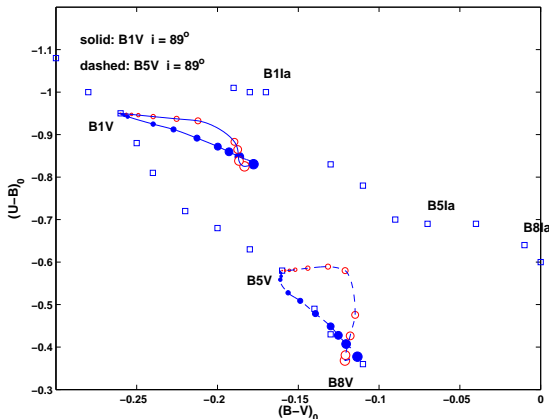


Figure 5. Same as Figure 2 but for edge-on disks seen at $i = 89^\circ$.

One feature of the reference models leading to the very small magnitude increase during edge-on observation is the very thin nature of the disks. Almost all calculations of Be star disks, either hydrodynamical or thermal/radiative, assume a geometrically thin disk with the scale height set by vertical hydrostatic equilibrium. As previously noted, this scale height is the ratio of the local sound speed to the local orbital speed. As Be star disks are relatively cool and the orbital speeds are Keplerian and large, the disk scale heights are predicted to be very small; near the star, the scale height is often only a few percent of the stellar radius. Some have questioned whether this assumption is really correct, and there is some circumstantial evidence to support enhanced inner disk scale heights (Arias et al. 2006; Zorec et al. 2007b).

To examine the sensitivity of the predicted magnitude changes to the inner disk scale height, we have adopted a simple model in which the disk scale height is not allowed to fall below a minimum value, $(H/R)_{\min}$, which we take to be 0.2. The effect on the disk scale height of the B1V model is shown in Figure 6. As can be seen, this assumption results in a disk of nearly constant scale height $(H/R) = 0.2$ until ≈ 30 stellar radii. Near the star, the implied scale height enhancement is a factor of ≈ 5 . Given this modification, the temperature structure of the disk, the H α EWs, and the optical UBV magnitudes and colours were recomputed.

One subtlety of the enhanced scale height models is that simply increasing the scale height over the reference model will result in disks that are more massive. To avoid this effect, we have reduced the ρ_0 of the enhanced models at each time in Table (2) by the amount required to match the disk mass of the reference model. Hence the disk mass of the enhanced scale height models as a function of time match those given in Figure 1. We note that the total emission measures of the disks now agree much better as well (within 30%). Another important effect of this reduction in ρ_0 is that the temperature structure of the enhanced scale height models are now much closer to those of the basic reference models. This is shown in Figure 7. Without the reduction in ρ_0 , the enhanced scale height model for B1V has a much more extensive inner cool zone in the equatorial plane as compared to the reference hydrostatic model. The enhanced scale height model with reduced ρ_0 shows much better agreement.

In this initial set of enhanced scale height calculations, we ignored gravitational darkening; this is potentially an important effect and it will be modelled in Section 4.4. Hence the results here can be used for Be stars rotating at less than $\approx 70\%$ of their critical velocity. Instead of presenting the entire sequence of models, as before for the reference models, we will focus solely on the correlation between the optical magnitude and H α equivalent width during the disk build sequence from 1 to 365 days.

The results are shown in Figure 8 for the B1V models and Figure 9 for the B5V models. The contrast with the reference hydrostatic models is striking. The thin, hydrostatic models show only a very small decrease in the brightness of the system while the enhanced scale height models clearly show strong inverse correlations for inclinations above about $\approx 75^\circ$. Perhaps the most significant difference is that increases in the visual magnitude of the system occur even for the largest values of

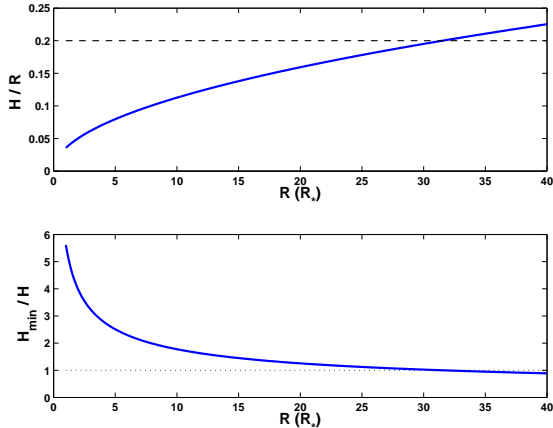


Figure 6. Top panel: hydrostatic scale height (Eq. 2) for the B1V model assuming $T_{HE} = 15\,000$ K. The scale height (H/R) at $1 R_*$ is predicted to be ~ 0.04 . $(H/R)_{\min} = 0.2$, adopted for some models in this work, is shown as the dashed line. Bottom panel: the disk scale height enhancement over the hydrostatic value obtained adopting a minimum value for (H/R) of 0.2. The dotted line is only a guide for the eye.

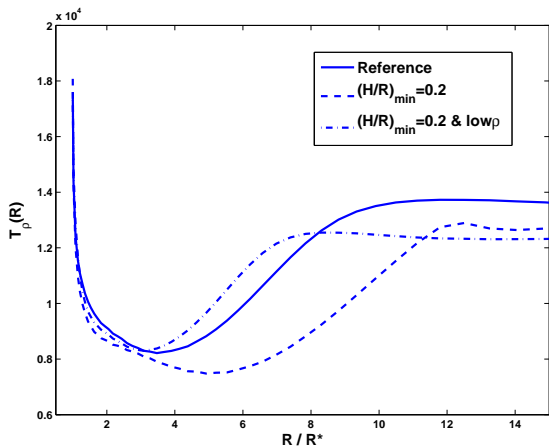


Figure 7. Comparison of the equatorial disk temperature between the reference B1V model (solid line) and a model with $(H/R)_{\min}$ set to 0.2 (dashed line). Also shown is the temperature structure of a $(H/R)_{\min} = 0.2$ model with ρ_0 reduced so that the total disk mass equals that of the reference B1V model (dash-dot line).

$H\alpha$ EW. In the pure hydrostatic models, all of the curves turn over at intermediate EW, and the system becomes brighter. From the enhanced scale height models, the dividing viewing inclination between positive and negative or inverse correlation is seen to be $\approx 75^\circ$. Hence the choice of $(H/R)_{\min} = 0.2$ seems to give an i_{crit} in agreement with the rough estimate of Section 2 based on the observed numbers of positive and negative correlations. Nevertheless, this should not be over interpreted; a more homogeneous sample of correlations coupled with detailed modelling of individual stars is required for a firm conclusion on enhanced disk scale heights for Be stars.

4.3. Alternate Disk Growth Models

One feature of the disk growth model implied by Eqs. (4) and (5) is that the disk density during the early growth phases, $t < 100$ days, is very low, and hence there is not a large impact on the system's spectral energy distribution. To see the effect of a much denser disk during

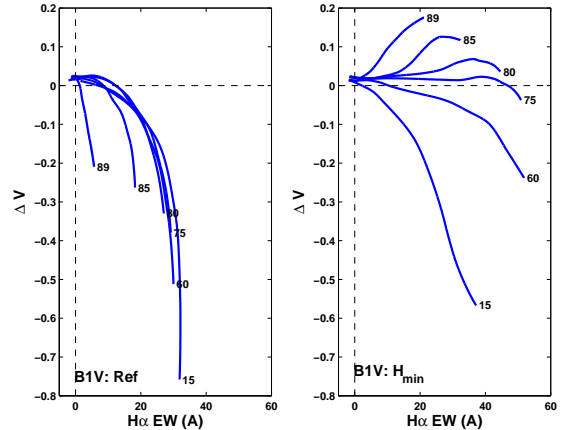


Figure 8. Relation between the change in V-magnitude and the $H\alpha$ equivalent during the disk building phase (1-365 days) for the B1V model. Each curve is labelled by the inclination of the system to the line of sight. The left panel shows the case of pure hydrostatic disks and the right panel shows the case of models with enhanced vertical scale heights.

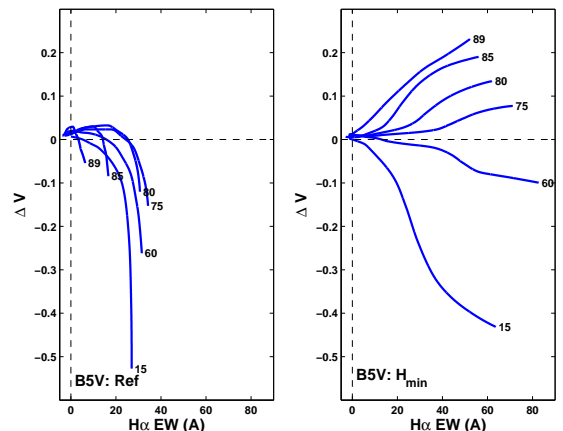


Figure 9. Same as Figure 8 except for the B5V model.

the early growth stages, we return to the two alternate disk growth assumptions outlined at the end of Section 3. Note that both of these alternate models assume a thin disk with the vertical scale height set by hydrostatic equilibrium via Eq. (2); these are not enhanced scale height models.

In the first alternate model with the base disk density set to a constant $\rho_o(t) = 10^{-10} \text{ g cm}^{-3}$, the outer radius of the disk simply grows with time. For this model, we have recalculated the change in V-magnitude and $H\alpha$ equivalent width during the growth phase ($t \leq 365$ days), and the results are shown in the left-hand panel of Figure 10 for the same viewing angles as the previous figures. As can be seen from the figure, the ΔV at early times is much larger because of the denser disk. The period of inverse correlation, however, is confined to the very initial times when the $H\alpha$ EW is still small. For later times, and larger values of the $H\alpha$ EW, the correlation flattens out and then turns over for all viewing angles. The case of the B5V model is shown in the left-hand panel of Figure 11 and is very similar to the B1V model, except that changes in the V magnitude are somewhat smaller.

In the second alternate disk growth model, a constant

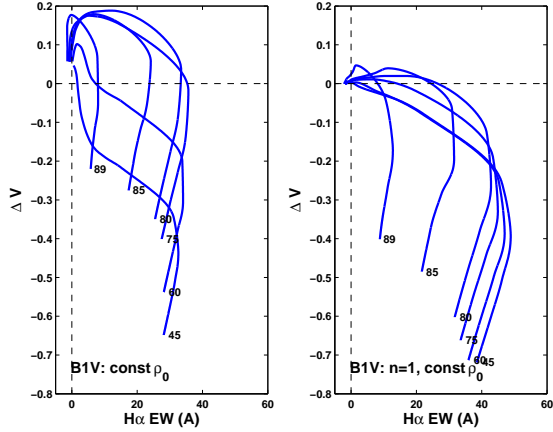


Figure 10. Same as Figure 8 for the B1V model but implementing the alternate disk growth scenarios of Section 4.3. The left panel is the constant ρ_0 disk, while the right panel has constant ρ_0 and $n = 1$ in the inner region.

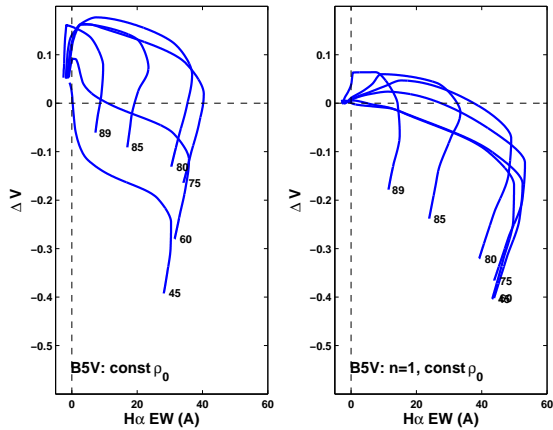


Figure 11. Same as Figure 10 but for the B5V model.

base disk density was again used, and in addition, a much shallower density drop-off in the equatorial plane for $R_d \leq 5 R_*$ was assumed by setting $n = 1$ in Eq. 1 over this range. To ensure that the fully built disk had the same mass as the previous models, the base disk density was taken to be a constant $\rho_o(t) = 2.7 \cdot 10^{-12} \text{ g cm}^{-3}$; the disk mass as a function of time is also shown in Figure 1. The results in the ΔV -H α diagram are shown in the right-hand panel of Figure 10 for the B1V model. In this case, weak inverse correlations are predicted for inclinations $i \geq 80^\circ$, but the dimming of the system is small, $\Delta V \approx 0.05 \text{ mag}$. In addition, like the previous case of $\rho_o(t) = 10^{-10} \text{ g cm}^{-3}$, the inverse correlation is confined to small H α EW; the relation flattens out and turns over into a positive correlation for larger EWs. A very similar result is obtained for the B5V model, as shown in the right-hand panel of Figure 11.

4.4. Gravitational Darkening

Be stars are known to be rapid rotators (Porter 1996; Yudin 2001), as first suggested by Struve (1931), although how close they are as a population to critical rotation is still uncertain (Townsend et al. 2004; Cranmer 2005; Meilland et al. 2012). Rapid rotation leads to gravitational darkening of the stellar surface in which the temperature varies with latitude, and the

shape of the star is no longer spherical. According to von Zeipel’s theorem (von Zeipel 1924), the local effective temperature should be proportional to the effective gravitational acceleration at each latitude, and this effect causes the equatorial regions of a rapidly rotating star to be much cooler than the poles. Gravitational darkening, both as the distortion of the stellar surface and as a variation of temperature over the stellar surface, now has ample, direct interferometric verification (van Belle 2012). These studies have led to the conclusion that while gravity darkening is present, von Zeipel’s theorem as applied to stellar atmospheres by Collins (1966) overestimates the temperature variation. Recently, Espinosa Lara & Rieutord (2011) have derived a new version of gravitational darkening that seems in better agreement with observations; we adopt their formalism.

Gravitational darkening is potentially an important effect in the current work, particularly for the case of an inverse correlation because the blocked equatorial region is now much cooler and hence fainter. One might expect that the size of the inverse correlation will depend on the extent of gravitational darkening.

We have used the formalism of Espinosa Lara & Rieutord (2011) to compute the variation of temperature with latitude over the stellar surface. Given the exploratory nature of the present calculations, however, we have neglected the distortion of the stellar surface. A useful term for this approximation is spherical gravitational darkening (SGD). We have also neglected the effect of gravitational darkening on the thermal structure of the circumstellar disk. This latter effect is extensively discussed by McGill et al. (2011) and even at critical rotation, the effect would be at most a 15% reduction in the average disk temperature.

Figure 12 shows the effect of SGD, with the central star rotating at 95% of its critical velocity, on the B1V model, both with a thin, hydrostatic disk (left panel) and the thicker $(H/R)_{\min} = 0.2$ disk (right panel). In the case of the thin, hydrostatic disk, almost all trace of the inverse correlation is gone. In the $(H/R)_{\min} = 0.2$ case, the inverse correlation is now seen only for higher inclinations ($i \geq 80^\circ$) and only for latter times in the disk-building process. A very similar result is seen in Figure 13 for the B5V model.

As a result, the existence of an inverse correlation depends strongly on the extent of gravitational darkening and hence, on the rotation rate of the central B star of the system. Note that these results would only contradict the existence of inverse correlations if all Be stars were rapid rotators. While the exact rotational distribution of Be stars remains unclear, it seems unlikely that all of them are critical rotators, at least for the earlier spectral types (Cranmer 2005).

5. DISCUSSION

In this work, simple parametrized models for Be star disk growth and dissipation are investigated to see if they can reproduce the known classes of positive and inverse correlations discovered by Harmanec (1983). We find that these simple models can demonstrate both positive and inverse correlations between the system’s change in visual magnitude and the magnitude of the H α emission. We also demonstrate the scale height of inner circum-

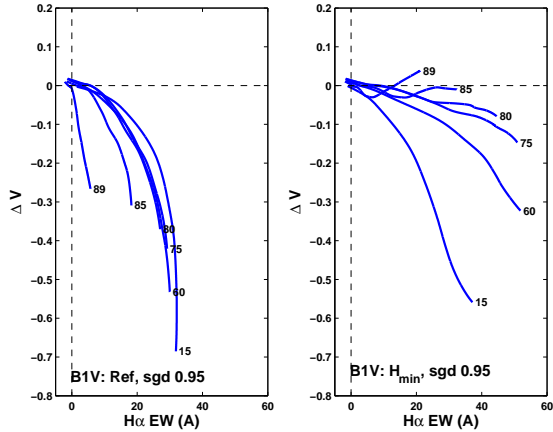


Figure 12. Same as Figure 8 for the B1V model but implementing spherical gravitational darkening assuming the star is rotating at 95% of its critical velocity.

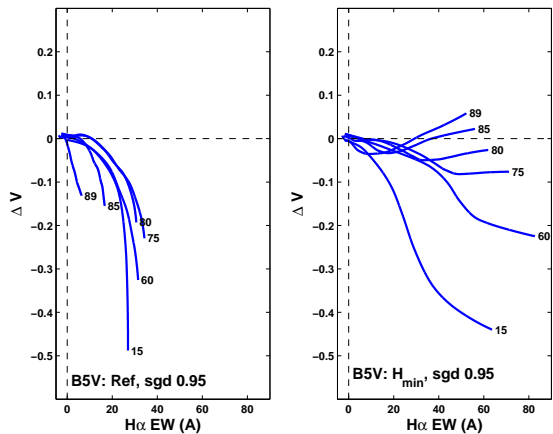


Figure 13. Same as Figure 12 but for the B5V model.

stellar disk and the extent of gravitational darkening of the central star's surface play key roles in controlling the magnitudes of the predicted correlations, particularly the inverse ones.

What do these calculations demonstrate? It is important to keep in mind that only parametrized, “toy” models of disk growth and dissipation were used, and hence it is difficult to draw general conclusions. However the calculations performed suggest that inverse correlations are more easily predicted for Be star disks with enhanced scale heights around B stars that are not significantly gravitationally darkened. Because the predicted correlations depend so strongly on these two aspects, gravitational darkening and disk scale height, it would be highly desirable to analyze a well determine set of contemporaneous magnitude and $H\alpha$ measurements through either a Be star growth or dissipation phase to determine to what extent the disk scale height and/or extent of gravitational darkening can be constrained. In the analysis of real observations, a much more realistic hydrodynamical description of disk growth would be preferable and such models are now available (e.g. Carciofi et al. 2012; Haubois et al. 2012).

This work is supported by the Canadian Natural Sciences and Engineering Research Council (NESRC)

through a Discovery Grant to TAAS. PP would like to thank J. D. Landstreet for additional financial support through his NSERC Discovery Grant. We thank J. D. Landstreet and Peter Harmanec for very helpful comments on the manuscript.

REFERENCES

- Andrilland, Y. 1983, *A&AS*, 53, 319
 Andrilland, Y., & Fehrehnbach, C. 1982, *A&AS*, 48, 93
 Arias, M. L., Zorec, J., Cidale, L., Ringuet, A. E., 2006, *A&A*, 460, 821
 Bagnulo, S., Landstreet, J. D., Fossati, L. & Kochukhov, O. 2012, *A&A*, 538, A129
 Baade, D., 2000 in *IAU Colloq. 175, The Be Phenomena in Early-Type Stars*, M. A. Smith, H. F. Henrichs, & J. Fabregat, eds., ASP Conf. Ser. 214, 178
 Baade, D., 1992 in *IAU Symp. 151, Evolutionary Processes in Interacting Binary Stars*, Y. Kondo et al., eds., 147
 Baade, D., & Balona, L. A. 1994 in *IAU Symp. 162, Pulsation, Rotation and Mass Loss in Early-Type Stars*, L. A. Balona, Henrichs, H. F., & Le Contel, J. M., Kluwer, Dordrecht, 311
 Balona, L. A., 2000 in *IAU Colloq. 175, The Be Phenomena in Early-Type Stars*, M. A. Smith, H. F. Henrichs, & J. Fabregat, eds., ASP Conf. Ser. 214, 1
 Barklem, P. S., & Piskunov, N. 2003 in *IAU Symp. 210, Modelling of Stellar Atmospheres*, ed. N. Piskunov, W. W. Wies, & D. F. Gray (San Francisco: ASP), E28
 Berio, P., Stee, Ph., Vakili, F., Mourard, D., Bonneau, D., Chesneau, O., Thureau, N., Le Mignant, D. & Hirata, R. 1999, *A&A*, 345, 203
 Bjorkman, J. E. & Cassinelli, J. P. 1993, *A&A*, 409, 429
 Božić, H., Harmanec, P., Horn, J., Koubsky, P., Scholz, G., McDavid, D., Hubert, A. -M, Hubert, H. 1995, 304, 235
 Božić, H., Ruždjak, D. & Sudar, D. 1999, *A&A*, 350, 566
 Božić, H., Harmanec, P., Yang, S., Žižňovský, J., Percy, J. R., Ruvdjak, D., Sudar, D., Šlechta, M., Škoda, P., Krpata, J. & Bul, C. 2004, *A&A*, 416, 669
 Carciofi, A. C., Bjorkman, J. E., Otero, Sebastián A., Okazaki, A. T., Steff, Stanislav, Rivinius, T., Baade, D., & Haubois, X. 2012, *ApJ*, 744, L15. Okazaki, A. T.,
 Carciofi, A. C. in *IAU Symposium 272, Active OB Stars: Structure, Evolution, Mass-Loss, and Critical Limits*, C. Neiner, G. Wade, G. Meynet, G. Peters eds., Cambridge University Press, 325
 Carciofi, A. C., Okazaki, A. T., Le Bouquin, J.-B., Šteff, S., Rivinius, Th., Baade, D., Bjorkman, J. E. & Hummel, C. A. 2009, *A&A*, 504, 915
 Cassinelli, J. P., Brown, J. C., Maheswaran, M., Miller, N. A., Telfer, D. C. 2002, 578, 951
 Clark, J. S., Tarasov, A. E. & Panko, E. A. 2003, *A&A*, 403, 239
 Chauville, J., Zorec, J., Ballereau, D., Morrell, N., Cidale, L. & Garcia, A. 2001, *A&A*, 378, 861
 Collins, G. W. II 1966, *ApJ*, 146, 914
 Coté, J., & Waters, L. B. F. M. 1987, *A&A*, 176, 93.
 Cox, A.N. 2000, *Allens Astrophysical Quantities* (4 th ed.; New York: Springer)
 Coyne, G. V. 1976, in *IAU Symposium No. 70, Be and Shell Stars*, ed. A. Slettebak, p. 233.
 Cranmer, S.R. 2009, *ApJ*, 701, 396
 Cranmer, S.R. 2005, *ApJ*, 634, 585
 Dachs, J., Stich, J., & Hanuschik, R. W., 1992, *A&AS*, 95, 437
 de Jager, C., & Nieuwenhuijzen, H., 1987, *A&A*, 177, 217
 Doazan, V., Harmanec, P., Koubsky, P., Krpata, J. & Zdarsky, F. 1982, *A&A*, 115, 138
 Doazan, V., Franco, M., Sedmak, G., Stalio, R. & Rusconi, L. 1983, *A&A*, 128, 171
 Dougherty, S. M., & Taylor, A. R. 1992, *Nature*, 359, 808
 Ekström, S., Meynet, G., Maeder, A., & Barblan, F., 2008, *A&A*, 478, 467
 Espinosa Lara, F., & Rieutord, M., 2011, *A&A*, 533, A43
 Evans, C. J. 2009 in *The Properties of early-type stars in the Magellanic Clouds*, ed. J. T. van Loon & J. M. Oliveira, IAU Symp. 256, 325
 Evans, C. J., & 25 co-authors, 2005, *A&A*, 437, 467

- Espinosa Lara, F. & Rieutord, M. 2011, A&A, 533, A43
- Fabregat, J., & Gutiérrez-Soto, J. 2005, Publ. Astron. Inst. ASCR, 93, 3
- Fabregat, J., & Torrejón, J. M. 2000, A&A, 357, 451.
- Fitzgerald, M. Pim. 1970, A&A, 4, 234
- Floquet, M., Hubert, A. M., Hirata, R., McDavid, D., Zorec, J., Gies, D., Hahula, M., Janot-Pacheco, E., Kambe, E., Leister, N. V., Štefl, S., Tarasov, A. & Neiner, C. 2000, A&A, 362, 1020
- Fremat Y., Zorec, J., Hubert, A.M., & Floquet M. 2 005, A&A, 440, 305
- Gehrz, R. D., Hackwell, J. A., & Jones, C. E. 1973, ApJ, 191, 675 ApJ, 654, 527
- Gies, D. R., and 24 co-authors 2007, ApJ, 654, 527
- Grundstrom, E. D., & Gies, D. R., 2007, ApJ, 651, 53
- Harmanec, P. 1983, Hvar Observatory Bulletin, 7, 115H
- Harmanec, P. 1998, A&A, 334, 558
- Harmanec, P. 1998, A&A, 341, 867
- Harmanec, P. 2000, IAU Colloquium 175, The Be Phenomena in Early-Type Stars, ASP Conference Series, Vol. 214, M. A. Smith, H. F. Henrichs, & J. Fabregat eds., 13
- Hanuschik, R. W., Hummel, W., Diette, O. & Sutorius, E. 1995, A&A, 300, 163
- Haubois, X., Carciofi, A. C., Rivinius, Th., Okazaki, A. T., & Bjorkman, J. E. 2012, ApJ, 756, 156
- Hill, G. M., Walker, G. A. H. & Yang, S. 1991, A&A, 246, 146
- Hill, G. M., Walker, G. A. H., Yang, S. & Harmanec, P. 1989, PASP, 101, 258
- Hirata, R., Shimada, M. R., Masuda, S. & Katahira, J. 2000, ASP Conference Series, 214, 558H
- Horn, J., Božić, H., Harmanec, P., Koubský, P., Pavlovski, K. & Žďárský, F. 1982, Bulletin Astronomy Institute Czechoslovakia (BAIC), 33, 308
- Huat, A.-L., and 21 co-authors 2009, A&A, 506, 95
- Hubert, H., Hubert, & Floquet, M., 1998, A&A, 335, 565
- Hubert, H., Hubert, A. M., Chatzichristou, H. & Floquet, M. 1990, A&A, 230, 131
- Hunter, I., and 7 co-authors 2008, A&A, 479, 541
- Hummel, W. & Hanuschik, R. W. 1997, A&A, 320, 8523
- Hummel, W., & Vrancken, M. 2000, A&A, 359, 1075
- Jaschek, M., Slettebak, A., & Jaschek, C. Be Star Newsl., No. 4, 9
- Johnson, H. J. 1966, ARA&A, 4, 193J
- Jones, C. E., Tycner, C., Sigut, T. A. A., Benson, J. A., & Hutter, D. J. 2008, ApJ, 687, 598
- Juza, K., Harmanec, P., Bozic, H., Pavlovski, K., Ziznovsky, J., Tarasov, A. E., Horn, J. & Koubsky, P. 1994, A&AS, 107, 403J
- Kurucz, R. F. 1993, Kurucz CD-ROM No. 13. Cambridge, Mass: Smithsonian Astrophysical Observatory
- Keller, S. C., Wood, P. R., & Bessell, M. S., 1999, A&AS, 134, 489
- Kogure, T. & Hirata, R. 1982, BASI, 10, 281
- Korn, A. J., Becker, S. R., Gummertsbach, C. A., & Wolf, B. 2000, A&A, 353, 655
- Koubsky, P., Harmanec, P., Kubt, J., Hubert, A. M., Boi, H., Floquet, M., Hadrava, P., Hill, G. & Percy, J. R. 1997, A&A, 328, 551-564
- Koubsky, P., Harmanec, P., Hubert, A. M., Floquet, M., Kubát, J., Ballereau, D., Chauville, J., Božić, H., Holmgren, D., Yang, S., Cao, H., Eenens, P., Huang, L. & Percy, J. R. 2000, A&A, 356, 913
- Krtička, J., Owocki, S. P., & Meynet, G. 2011, A&A, 527, A84
- Lanz, T. & Hubeny, I. 2007, ApJS, 83, 104.
- Lee, U., Saio, H., & Osaki, Y. (1999), MNRAS, 250, 342
- Maeder, A., Grebel, E. K., & Mermilliod, J.-C. 1999, A&A, 346, 559
- Maeder, A. & Meynet, G. 2001, A&A, 373, 555
- Mathew, B., Subramaniam, S., & Bhatt, B. C. 2008, MNRAS, 388, 1897
- Martayan, C., Baade, D., & Fabregat, F. 2010, A&A, 509, A11.
- Martayan, C., Frémat, Y., Hubert, A.-M., Floquet, M., Zorec, J., & Neiner, C. 2007, A&A, 462, 683
- Martayan, C., Floquet, M., Hubert, A.-M., Gutiérrez-Soto, J., Fabregat, J., Neiner, C., & Mekkas, M. 2007, A&A, 472, 577
- Martayan, C., Frémat, Y., Hubert, A.-M., Floquet, M., Zorec, J., & Neiner, C. 2006, A&A, 452, 273
- McGill, M. A., Sigut, T. A. A., & Jones, C. E. 2012, ApJS, 204, 2
- McGill, M. A., Sigut, T. A. A., & Jones, C. E. 2011, ApJ, 743, 111
- McLean, I. S., & Brown, J. C., 1978, A&A, 69, 291
- McSwain, M.V., & Gies, D.R. 2005, A&AS, 161, 118
- McSwain, M. V., & Gies, D. R. 2005, ApJ, 662, 1052
- Melliand, A., Stec, Ph., Zorec, J. & Kannan, S. 2006, A&A, 455, 953
- Meilland, A., Stee, Ph., Chesneau, O., & Jones, C. 2009, A&A, 505, 687.
- Meilland, A., Millour, F., Kanaan, S., Stee, Ph., Petrov, R., Hofmann, K.-H., Natta, A., & Perraut, K. 2012, A&A, 538, A110
- Mihalas, D. 1978 *Stellar Atmospheres* (W. H. Freeman & Company: New York)
- Millar, C. E., & Marlborough, J. M. 1998, ApJ, 494, 715
- Mokiem, M. R., and 11 co-authors, 2007, A&A, 473, 603.
- Mourard, D., Bosc, I., Labeyrie, A., Koechlin, L. & Saha, S. 1989, Nature, 342, 520
- Nordh, H. L. & Olofsson, S. G. 1977, A&A, 56, 117
- Okazaki, A. T. 1991, PASP, 43, 75
- Okazaki, A. T. 1997, A&A, 318, 548
- Osaki, Yoji, 1999 in IAU Colloq. 169, Variable and Non-Spherical Winds in Luminous Hot Stars, B. Wolf, O. Stahl, & A. Fullerton, eds., Lecture Notes in Physics, 523, 329
- Oudmajer, R., Parr, A.M., Baines, D., & Porter, J.M. 2008, A&A, 489, 627
- Pavlovski et al. 1983, IBVS, 2431, 1P
- Penny, L. R., Sprague, A. J., Seago, G., & Gies, D. R. 2004, ApJ, 617, 1316
- Peters, G. J. 1986, ApJ, 301, L61
- Poeckert, R., Bastien, P., & Landstreet, J. D. 1979, AJ, 84, 812
- Porter, John M., & Rivinius, T. 2003, PASP, 115, 1153
- Porter, John M. 1999 A&A, 348, 512
- Porter, John M. 1996 MNRAS, 280, L31
- Quirrenback, A., & 8 co-authors, ApJ, 479, 477
- Quirrenback, A., Hummel, C. A., Buscher, D. F., Armstrong, J. T., Mozurkewich, D., Elias II, N. M. & Babler, B. L. 1993, ApJ, 416, L25
- Rivinius, Th., Baade, D., Stefl, S. & Maintz, M. 2001, A&A, 379, 257
- Rivinius, Th., Baade, D., Štefl, S., Townsend, R. H. D., Stahl, O., Wolf, B. & Kaufer, A. 2001b, A&A, 369, 1058
- Rivinius, T., Baade D., Stefl, S., Stahl, O., Wolf, B., & Kaufer, A., 1998, A&A, 336, 177
- Rivinius, Th., Baade, D., Štefl, S. et al. 1998a, A&A, 333, 125
- Rivinius, Th. Baade, D., Stefl, S. et al. 1998b, in Cyclic variability in stellar winds, Kaper, L. & Fullerton, A., ESO Conference Series, 207
- Rolleston, W. R., Venn, K., Tolstoy, E., Dufton, P. L. 2003, A&A, 400, 21
- Saad, s. M., Kubát, J., Koubský, P., Harmanec, P., Škoda, P., Korčáková, D., Krtička, J., Šlechta, M., Božić, H., Ak, H., Hadrava, P. & Votruba, V. 2004, A&A, 419, 607
- Sareyan, J. P., Gonzalez-Bedolla, S., Guerrero, G., Chauville, J., Huang, L., Hao, J. X., Guo, Z. H., Adelman, S. J., Briot, D. & Alvarez, M. 1998, A&A, 332, 155
- Sigut, T.A.A. 2011 IAU Symp. 272, "Active OB Stars: Structure, Evolution, Mass-Loss, and Critical Limits," Neiner, C., Wade, G., Meynet, G., & Peters, G. (eds), 426
- Sigut, T.A.A, McGill, M.A., Jones, C.E. 2009, ApJ, 699, 1973
- Sigut, T.A.A, & Jones, C.E. 2007, ApJ, 668, 481
- Slettebak, A. 2007, PASP, 100, 770
- Stee, P., 2011, in IAU Symp. 272, "Active OB Stars: Structure, Evolution, Mass-Loss, and Critical Limits," Neiner, C., Wade, G., Meynet, G., & Peters, G. (eds), 313
- Stee, P., de Araujo, F. X., Vakili, F., Mourard, D., Arnold, L., Bonneau, D., Morand, F. & Tallon-Bosc, I. 1995, A&A, 300, 219
- Štefl, S., Baade, D., Rivinius, Th., Otero, S., Stahl, O., Budovičová, A, Kaufer, A., & Maintz M. 2003, A&A, 402, 253
- Štefl, S., Baade, D., Harmanec, P. & Balona, L. A. 1995, A&A, 294, 135
- Struve, Otto 1931, ApJ, 73, 94
- Harmanec, P. & Balona, L. A. 1995, A&A, 294, 135
- Tanaka, K., Sadakane, K., Narusawa, S., Naito, H. & Kambe, E. 2007, PASJ, 59, L35
- Tarasov, A. E., & Malchenko, S. L. 2012, Astro. Let., 38, 428
- Thom, C., Granes, P. & Vakili F. 1986, A&A, 165, L13
- Townsend, R. H. D., Owocki, S. P., & Howarth, D. 2004, MNRAS, 350, 1989
- Trundel, C., and 6 co-authors, 2007, A&A, 471, 625.

- Tycner, C., Jones, C., Sigut, T. A. A., Scmitt, H. R., Benson, J. A., Hutter, D. J., & Zavala, R. T. 2008, *ApJ*, 689, 461
- Tycner, C., and 8 co-authors 2005, *ApJ*, 624, 359
- van Belle, G. T. 2012, *A&ARv*, 20, 51
- Van Bever, J. & Vanbeveren, D. 1997, *A&A*, 322, 116.
- Vakili, F., Mourard, D., Stee, Ph., Bonneau, D., Berio, P., Chesneau, O., Thureau, N., Morand, F., Labeyrie, A. & Tallon-Bosc, I. 1998, *A&A*, 335, 261
- Vink, J. S., de Koter, A., & Lamers, H. G. J. L. M. 2001, *A&A*, 369, 574
- von Zeipel, H. 1924, *MNRAS*, 84, 665
- Wisniewski, J. P., Draper, Z. H., Bjorkman, K. S., Meade, M. M., Bjorkman, J. E., & Kowalski, A. F. 2010, *ApJ*, 709, 1306
- Wisniewski, J.P., & Bjorkman, K.S. 2006, *ApJ*, 652, 458
- Wade, R.A., & Rucinski, S.M. 1985, *A&AS*, 471, 484
- Yudin, R. V., 2001, *A&A*, 368, 912
- Zorec, J., & Briot, D. 1997, *A&A*, 318, 443
- Zorec, J., Arias, M. L., Cidale, L., & Ringuelet, A. E., 2007, *A&A*, 470, 239